JCB Journal of Cell Biology

ARTICLE

# Coronin 1A depletion restores the nuclear stability and viability of Aip1/Wdr1-deficient neutrophils

Charnese Bowes[1,2*], Michael Redd[3*], Malika Yousfi[1,2*], Muriel Tauzin[1,2], Emi Murayama[1,2], and Philippe Herbomel[1,2]

**Actin dynamics is central for cells, and especially for the fast-moving leukocytes. The severing of actin filaments is mainly achieved by cofilin, assisted by Aip1/Wdr1 and coronins. We found that in Wdr1-deficient zebrafish embryos, neutrophils display F-actin cytoplasmic aggregates and a complete spatial uncoupling of phospho-myosin from F-actin. They then undergo an unprecedented gradual disorganization of their nucleus followed by eruptive cell death. Their cofilin is mostly unphosphorylated and associated with F-actin, thus likely outcompeting myosin for F-actin binding. Myosin inhibition reproduces in WT embryos the nuclear instability and eruptive death of neutrophils seen in Wdr1-deficient embryos. Strikingly, depletion of the main coronin of leukocytes, coronin 1A, fully restores the cortical location of F-actin, nuclear integrity, viability, and mobility of Wdr1-deficient neutrophils in vivo. Our study points to an essential role of actomyosin contractility in maintaining the integrity of the nucleus of neutrophils and a new twist in the interplay of cofilin, Wdr1, and coronin in regulating F-actin dynamics.**

## Introduction

The turnover of actin filaments (F-actin) is essential for the highly mobile leukocytes. As F-actin is a stable polymer, its turnover requires molecular machineries to polymerize and depolymerize or sever actin filaments in a spatially and temporally coordinated manner within the cell. Several protein complexes driving F-actin polymerization in colinear or variously branched configurations have been identified (Blanchoin et al., 2014). F-Actin severing is mainly accomplished by small proteins, the cofilins, with the help of facilitating cofactors, the best known of which are Aip1 (actin interacting protein 1, also called Wdr1 due to its primary and tertiary structure; Ono, 2018) and the coronins (Bamburg et al., 1999; Andrianantoandro and Pollard, 2006; Cai et al., 2007; Gandhi and Goode, 2008; Brieher, 2013; Gressin et al., 2015). Cofilins bind somewhat cooperatively to F-actin, and F-actin severing by cofilin alone occurs at boundaries between cofilin-covered and bare F-actin. F-Actin filaments fully covered by cofilin lack such boundaries and are therefore stabilized rather than severed (Andrianantoandro and Pollard, 2006). Wdr1 is able to bind cofilin-loaded F-actin and induce their rapid severing (Nadkarni and Brieher, 2014). Recent studies have shown that, among other modes of action (Galkin et al., 2001; Cai et al., 2007; Gandhi and Goode, 2008), coronin binding to F-actin facilitates the further binding of cofilin and subsequent F-actin severing (Jansen et al., 2015). However, since most of these results are from experiments using in vitro assays, the extent to which they represent actin dynamics in the highly mobile leukocytes remains to be assessed. Cofilins, coronins, and Wdr1 are highly expressed in neutrophils (Singh et al., 2013b; Fagerberg et al., 2014). Among leukocytes, neutrophils appear to be especially sensitive to perturbations of their actin dynamics, which can even compromise their viability. For example, X-linked congenital neutropenia in humans is due to an activating mutation in Wiskott-Aldrich syndrome protein (WASp), a protein fostering F-actin polymerization that is expressed in all leukocytes. Yet this mutation, which expectedly causes F-actin excess in all leukocytes, is lethal only for the neutrophils (Moulding et al., 2007, 2012). Other inherited human immunodeficiencies have been described that are mainly due to defective neutrophil migration to infection sites. Such is the case for several neutrophil cytoskeletal diseases (Nunoi et al., 2001), including the lazy leukocyte syndrome (LLS; Miller et al., 1971; Goldman et al., 1984), in which the mainly cortical (i.e., sub-plasmalemmal) location of F-actin is replaced by F-actin aggregates in the

[1]Institut Pasteur, Department of Developmental and Stem Cell Biology, Paris, France; [2]Centre National de la Recherche Scientifique, UMR3738, Paris, France; [3]University of Utah, Huntsman Cancer Institute, Salt Lake City, UT.

*C. Bowes, M. Redd, and M. Yousfi contributed equally to this paper; Correspondence to Philippe Herbomel: philippe.herbomel@pasteur.fr; M. Redd's present address is Cell and Developmental Biology, University College London, London, UK; M. Tauzin's present address is Centre Hospitalier Universitaire de Toulouse, Direction de la Recherche Médicale et de l'Innovation, Toulouse, France.

cytoplasm. Several LLS cases were recently shown to be due to mutations in WDR1 (Kuhns et al., 2016; Pfajfer et al., 2018). However, these cytoskeletal defects are difficult to study since human (or mouse) neutrophils are very short lived in cell culture.

Due to its transparency and very small size, the developing zebrafish has become an attractive vertebrate model to study the biology of neutrophils in vivo, down to subcellular resolution (Le Guyader et al., 2008; Yoo et al., 2010, 2012; Sarris et al., 2012; Shelef et al., 2013). In a forward genetic screen for neutropenic zebrafish, we isolated a Wdr1-deficient mutant, in which neutrophils are initially produced in the embryo, but then quickly decline and disappear. We found that beyond their perturbed actin dynamics and motility, neutrophils undergo an unexpected disintegration of their nuclear envelope (NE), preceding their death. This nuclear phenotype is phenocopied in WT embryos by a mere inhibition of actomyosin contractility. Conversely, the deleterious effects of Wdr1 deficiency on the neutrophils are entirely rescued by depletion of their major coronin, coronin 1A. Our results altogether uncover vital interactions between cofilin, Wdr1, coronin, and actomyosin contractility in neutrophils in vivo. They also open a new prospect for the future treatment of LLS patients.

## Results

### Wdr1 is essential for the maintenance of neutrophils in developing zebrafish

An *N*-ethyl-*N*-nitrosourea mutagenesis screen for recessive mutations causing neutropenia in zebrafish swimming larvae led to the identification of a mutant, which we called *carmin*, that had no neutrophils while displaying otherwise normal overall morphology (Fig. 1 A). High-resolution positional mapping identified the mutated gene as *wdr1*. Corroborating this, a *wdr1* retroviral insertion mutant from the Hopkins collection (Amsterdam et al., 2004) failed to genetically complement *carmin* (Fig. S1), and two morpholinos designed against *wdr1* RNA reproduced the carmin phenotype in WT embryos (Fig. 1 D), indicating that the *carmin* allele acts as a Wdr1 deficiency. The *wdr1* gene encodes a protein containing 14 WD40 repeats that fold into two β-propeller domains, each consisting of seven blades (Voegtli et al., 2003; Ono, 2018). The *carmin* allele comprises a T-to-C transversion, causing the substitution of a tryptophan residue conserved from yeast to human into an arginine in the C-terminal WD40 repeat of the protein (Fig. 1 C).

We transferred the *carmin* allele into transgenic backgrounds highlighting neutrophils—Tg(mpx:GFP), Tg(lyz:GFP), or Tg(lyz:DsRed)—to track the impact of Wdr1 deficiency on neutrophil fate in live developing embryos. Neutrophil counts following confocal microscopy of live embryos over time confirmed that *carmin* embryos were initially able to effectively produce neutrophils, but neutrophil number then steadily declined, such that by 72 h postfertilization (hpf) *carmin* larvae had <10% of the WT neutrophil population (Fig. 1 B and Video 1).

### Wdr1 deficiency causes systemic aggregation of actin and nuclear instability in neutrophils

Wdr1/Aip1 is known as a cofactor of cofilin, the main effector of F-actin depolymerization (Ono, 2003, 2018). We therefore combined the detection of neutrophils and of F-actin in mutant and sibling embryos and larvae. Wdr1 deficiency led to the accumulation of F-actin in the carmin mutant. These F-actin aggregates were first seen by 52 hpf in neutrophils as intracytoplasmic clumps and in the caudal fin epidermis as excess cortical actin (Fig. 2, A and B). Then over the next few days they progressively accumulated throughout the body, notably the epidermis and epithelial tubes (gut, pronephric ducts, and tubules; Fig. S2), with concomitant spreading of edema until death by 8–10 d postfertilization (dpf).

To observe the dynamics of F-actin in the neutrophils of mutant versus sibling embryos, we performed time-lapse confocal imaging of Tg(mpx:GFP) embryos injected with a plasmid driving expression of the F-actin reporter Lifeact-Ruby in neutrophils (Yoo et al., 2010). *Carmin* neutrophils harbored intense F-actin clumps that remodeled only slowly in contrast with the neutrophils of sibling embryos that showed the classic enrichment in F-actin at the cell cortex and at transient smaller foci associated with their fast amoeboid motility (Fig. 2 C and Video 2).

Whole-mount Hoechst 33342 staining of DNA in fixed embryos revealed that carmin neutrophils seemed to have multiple small abnormal nuclei (Fig. 3 A and Video 3). However, live confocal imaging of neutrophil nuclei in Tg(mpx:GFP) embryos transiently expressing a Lyz:H2b-mCherry transgene (Yoo et al., 2012) revealed nuclear lobules that were actually joined by unraveled and thinly stretched threads of chromatin (Fig. 3 B and Video 5). Concordantly, centrosome staining via γ-tubulin antibody revealed only one centrosome per neutrophil examined (Fig. S3), excluding centrosome amplification and aneuploidy. Given that the nuclei of WT zebrafish larval neutrophils, unlike those of humans, are not multilobulated, this indicated that $Wdr1^{-/-}$ neutrophils undergo nuclear dysmorphology.

To examine this phenomenon dynamically, we conducted time-lapse confocal imaging of Tg(mpx:GFP) embryos transiently expressing the Lyz:H2b-mCherry transgene to specifically highlight the chromatin of neutrophils (Videos 4, 5, and 6). These time-lapse sequences revealed a striking characteristic, wherein the chromatin of $wdr1^{-/-}$ neutrophils appeared to continuously unravel and unwind over the course of 5–10 h within the intact cell, until it suddenly condensed in discrete clumps within an hour, and the cell then most often erupted into fragments (Fig. 3 B and Video 5).

The final eruption of *carmin* neutrophils indicated a cell death mode quite different from classic neutrophil apoptosis seen in mammals and zebrafish (Fox et al., 2010; Loynes et al., 2010), wherein the cell merely shrinks (then optionally inflates, reflecting secondary necrosis) before death. Consistently, only a small proportion of neutrophils (5% by 54 hpf) in live *carmin* embryos had their surface labeled with fluorescent annexin V, indicating that carmin neutrophils for the most part do not die by apoptosis. A greater percentage of neutrophils were marked by a TUNEL assay (25% at 54 hpf and 37% at 72 hpf), indicative of DNA double-strand breaks, and this always correlated with a more intense staining by Hoechst 33342, indicative of DNA condensation, and with exclusion of GFP from this condensed chromatin (Fig. 3 C; $n = 24$). Together with the in vivo time-lapse

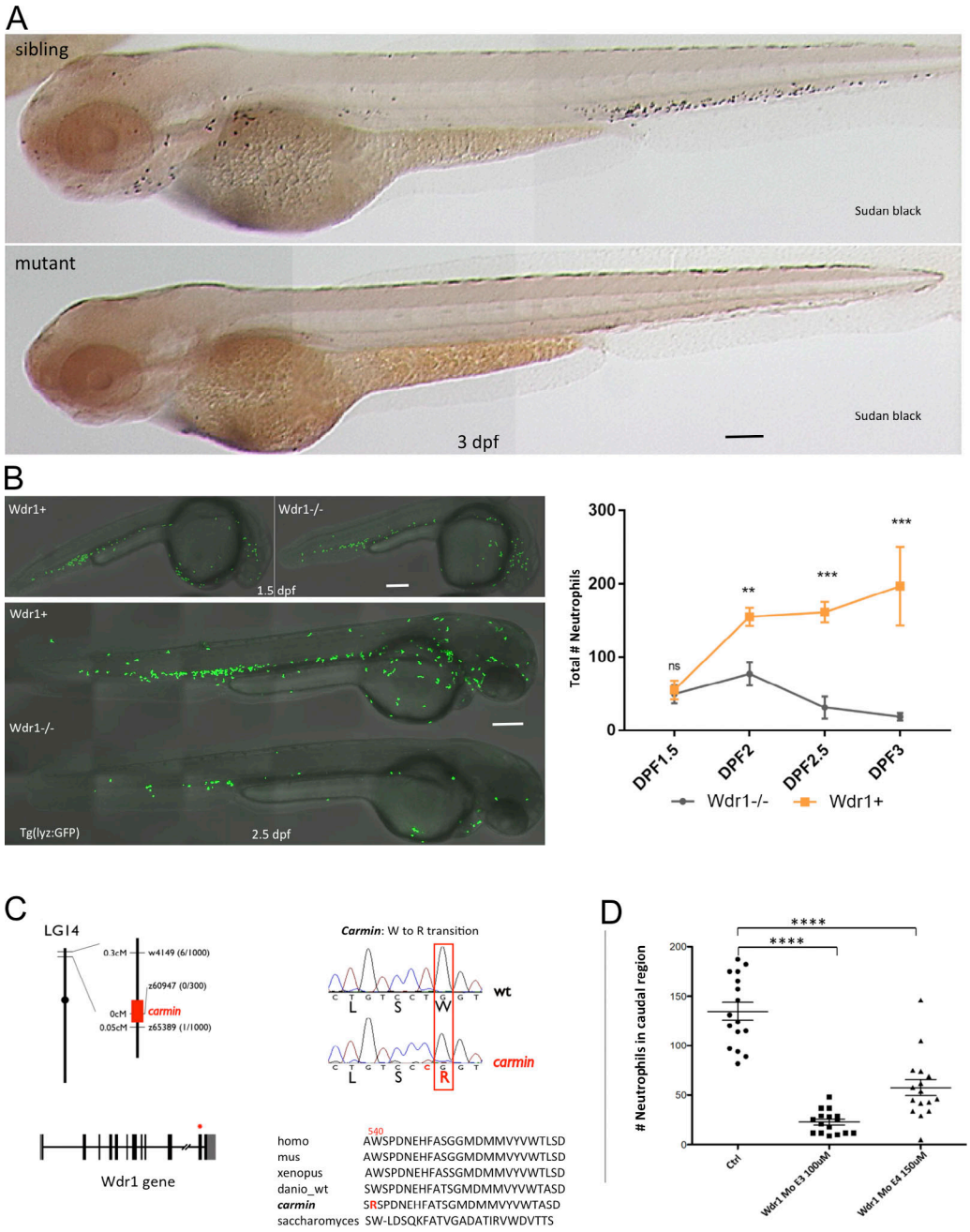


Figure 1. **Wdr1 is necessary for the maintenance of neutrophils in developing zebrafish. (A)** Sudan black–stained 3-dpf *carmin* embryos and siblings reveal a large reduction in neutrophils in carmin mutants. Scale bar, 100 µm. **(B)** 50 live *Tg(lyz:GFP) carmin* and sibling embryos were imaged by confocal fluorescence microscopy (left), and the total number of neutrophils was counted in a subset at several stages between 1.5 dpf/36 hpf and 3 dpf/72 hpf (right). Statistical significance of the difference between mutant and sibling embryos was determined by one-way ANOVA, with Sidak's multiple comparisons test; not significant (ns), $P > 0.05$; **, $P \le 0.01$; ***, $P \le 0.001$. Data shown as mean ± SD. Scale bar, 200 µm. **(C)** Mutation mapping (left) and subsequent sequence analysis (right) revealed a W-to-R substitution at position 540, close to the C terminus of Wdr1. **(D)** Number of neutrophils at 56 hpf in the caudal half (from midtrunk to tail tip) of WT embryos injected with either of two splice-blocking morpholinos against Wdr1 ($n = 16$ for each category), all from the same experiment (no pooling); this experiment was repeated at least four times. Data are mean ± SEM. ****, $P < 0.0001$ with two-tailed unpaired *t* test .

imaging data, this suggests that the neutrophil chromatin is able to unwind extensively for hours within the live cell, until double-strand DNA breaks occur (as detected by TUNEL) and trigger chromatin condensation, followed by cell fragmentation.

Concordantly, neighboring and still-functional macrophages were not attracted to the neutrophils while their nucleus unwound for hours. They bypassed the neutrophils in this state and approached and engulfed them only after the latter had passed through the chromatin condensation phase (Video 6). This was compelling evidence that the mutant neutrophils do not secrete or expose death signals at their surface until the ultimate phase of DNA breaks and condensation. Hereafter we

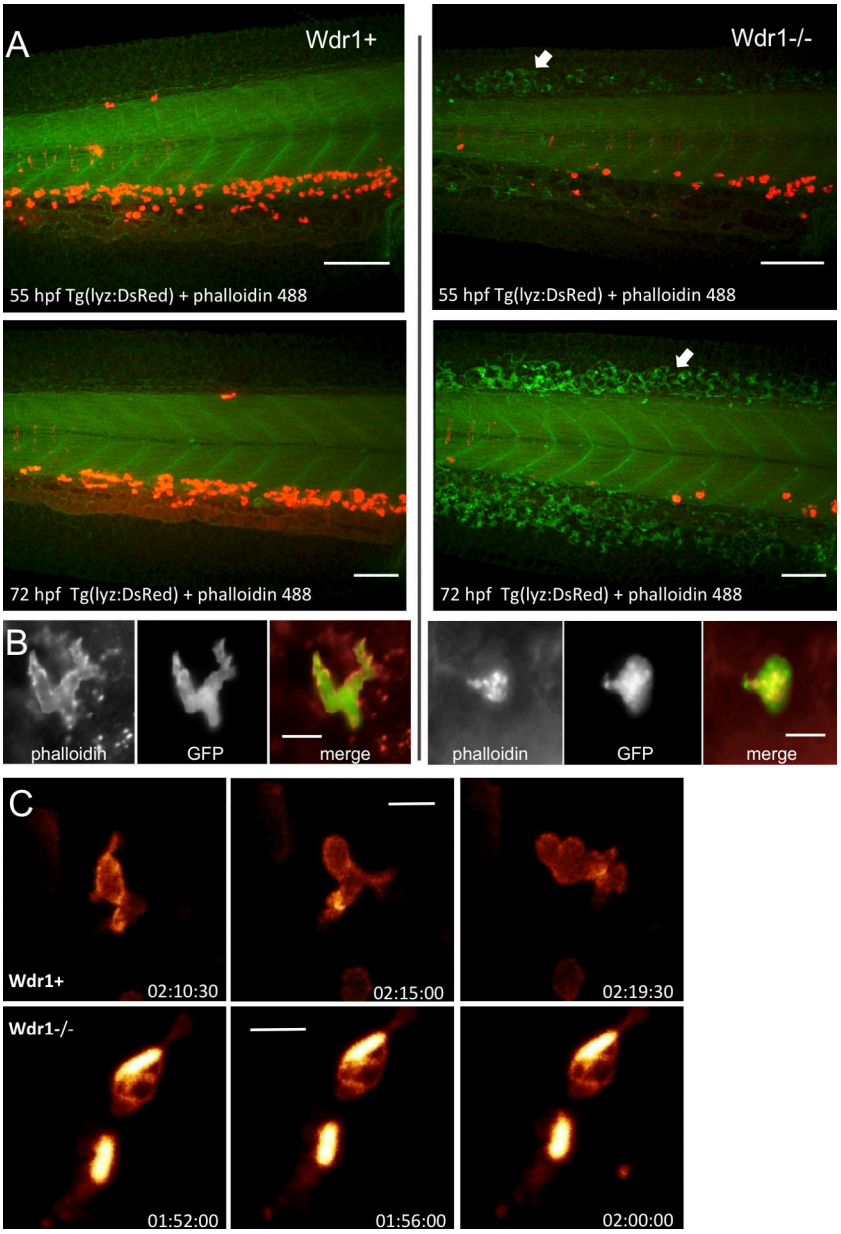


Figure 2. **Wdr1 deficiency leads to the accumulation of F-actin in the *carmin* mutant. (A)** F-Actin (green) and neutrophils (red) in the tail of Wdr1$^{carmin}$ versus Wdr$^{+}$ sibling embryos (dorsal up and rostral to the right); arrows point at cortical/subcortical F-actin aggregates in epidermal cells of the caudal fin in mutant embryos. **(B)** F-Actin in neutrophils. In WT neutrophils, F-actin is observed diffuse in the cytoplasm and delineating the cell cortex, whereas in the mutant it accumulates as intracytoplasmic clumps. **(C)** Time-lapse confocal imaging of Tg(mpx:GFP) *carmin* and WT sibling embryos injected with a mpx:Lifeact-ruby plasmid also reveal intense and only slowly remodeling F-actin clumps in the mutant neutrophils; time is indicated in h:min:s (see also Video 2). Scale bars, 100 µm (A) and 10 µm (B and C).

will call "late" the stage of mutant neutrophil pathology at which chromatin has become condensed, GFP depleted, and TUNEL positive, and "early" any stage before that.

### The nuclear lamina becomes disrupted in Wdr1-deficient neutrophils

We hypothesized that the unraveling of chromatin in mutant neutrophils might be due to disruption of the NE. NE disruptions typically occur at gaps in the nuclear lamina, a meshwork of intermediate filament proteins, the lamins, that connect the chromatin to the inner nuclear membrane (Hatch, 2018). As lamin A is known to be virtually absent in neutrophils (at least in mammals; Olins et al., 2008; Rowat et al., 2013), we immunodetected lamin B2 in whole embryos.

In sibling embryos, while the lamin B immunodetected in neutrophils was lower than in other cell types, in agreement with the literature (Olins et al., 2008), it did delineate the NE (Fig. 4 A). In contrast, about half of the mutant neutrophils displayed no lamin B–delineated NE (Fig. 4, B–E), but lamin B aggregates (Fig. 4 D), or no lamin B signal (Fig. 4, B and C). No mutant neutrophil at the late stage showed a lamin B–delineated NE ($n$ = 18; Fig. 4, C, D, and F). The lack of lamin B–delineated NE was also found in a fraction (two of nine) of mutant neutrophils at the early stage (Fig. 4 B and Video 7).

### Perturbation of actomyosin contractility (re)produces chromatin unwinding in neutrophils

How could Wdr1 deficiency cause the disruption of the nuclear lamina observed in mutant neutrophils? The physiological breakdown of the nuclear lamina during the cell cycle is achieved by phosphorylation of the lamins, notably via CDK1 (Ungricht and Kutay, 2017). To test if the mutant nuclear phenotype was due to an inappropriate induction of CDK1, we treated mutant embryos from 2 dpf onwards with a CDK1

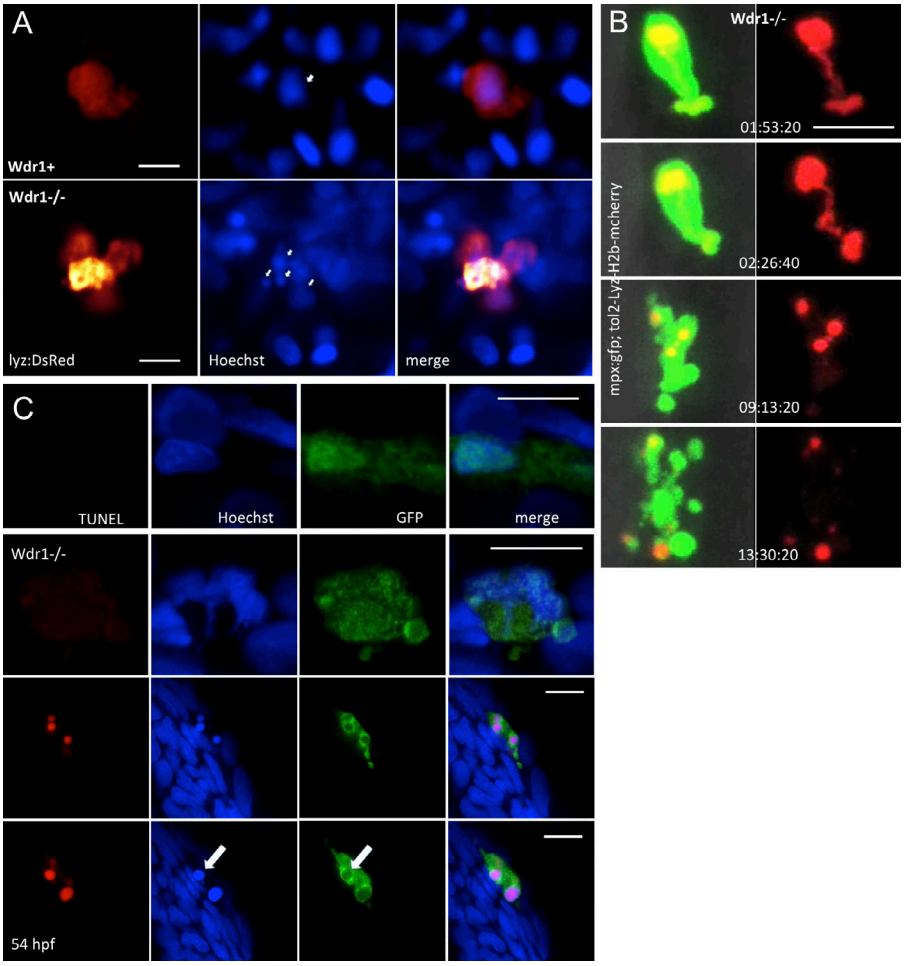


Figure 3. **Unusual characteristics of the Wdr1-deficient neutrophil nucleus. (A)** Hoechst staining of Tg(lyz:DsRed) embryos reveals that unlike WT, mutant neutrophils display a multiglobular nucleus. **(B)** Time-lapse imaging of Lyz:H2b-mCherry in Tg(mpx:GFP) mutant embryos documents a striking, continuous unraveling of the chromatin of neutrophils over the course of 9 h, after which chromatin rapidly condenses in several clumps and the cell erupts; see also Videos 4, 5, and 6. **(C)** TUNEL staining of mutant versus WT GFP$^+$ neutrophils by 54 hpf. The second row shows a mutant neutrophil with an already deformed nucleus, but no TUNEL staining, nor GFP depletion from the nucleus ($n$ = 6). 25% of mutant neutrophils are TUNEL$^+$ by then; the third and fourth rows show an example (two confocal planes of the same neutrophil); in this case, the nucleus appears multiglobular. Each globule is TUNEL$^+$ and also displays enhanced Hoechst staining due to DNA condensation and GFP depletion relative to the cytoplasm (arrow; $n$ = 24). Scale bars, 10 µm.

inhibitor previously validated in zebrafish embryos, RO-3306 (Strzyz et al., 2015). This treatment did not rescue the mutant neutrophils. Then, since mutant neutrophils displayed abnormal actin organization and dynamics, we wondered if actomyosin contractility might be perturbed. So we examined the distribution of active myosin versus F-actin in neutrophils of *carmin* versus sibling embryos at 2.5 dpf by whole-mount immunodetection of Ser19-phosphorylated myosin light chain (pMLC). This revealed, only in the mutant neutrophils, areas of intense pMLC staining which seemed to "cap" or form thick peripheral bands around the cell (Fig. 5, A and B), in positions quite apart from the F-actin clumps, suggesting an unusual spatial uncoupling of pMLC and F-actin, which would compromise actomyosin contractility. Interestingly, quantification via 3D image analysis of neutrophils segmented from the tissue by their GFP content showed that mutant neutrophils had pMLC and F-actin mean densities similar to those of WT sibling embryos (Fig. 5 C), indicating that their prominent F-actin clumps and pMLC caps actually reflected only a local and not a global excess of F-actin and pMLC in the cell.

We examined the spatial uncoupling of F-actin and pMLC more systematically by quantifying their degree of colocalization within individual neutrophils in mutant versus sibling embryos (Fig. 5 D). In WT neutrophils, F-actin and pMLC showed a substantial degree of colinear variation (Pearson coefficient = 0.40) and colocalization (Manders' coefficient A = 0.63 and B = 0.52; see Fig. 5 legend). In sharp contrast, all three coefficients collapsed in the mutant neutrophils; the Pearson coefficient actually collapsed to a mean value of zero (0.0047), and even to a negative value (meaning anticorrelation) for 6 of 12 cells. Even the two cells in this series that showed the highest (even though still lower than the WT mean) Pearson and Manders' correlations displayed a prominent peripheral pMLC cap (Fig. 5 B). This analysis thus uncovered a striking uncoupling of pMLC and F-actin localization throughout the mutant neutrophils, which necessarily precedes the unwinding of the nucleus, since we found it in all mutant neutrophils that we examined, either as peripheral pMLC caps and/or as a fine-grained decorrelation of pMLC and F-actin.

Based on these results, we investigated whether pharmacological perturbation of actomyosin contractility in WT neutrophils might reproduce, in part or in full, the phenotype of Wdr1-deficient neutrophils. To this aim, we used Rockout, a Rho kinase inhibitor reportedly more efficient in zebrafish embryos than the Y-27632 more widely used for mammalian cells (Weiser and Kimelman, 2012) to reduce actomyosin contractility by inhibiting MLC Ser19 phosphorylation (Maekawa et al., 1999; Wiggan et al., 2012). Incubation of 2 dpf WT Tg(mpx:GFP; Lyz:H2b-mCherry) embryos with Rockout for 8–16 h appeared compatible with embryo viability. It reduced the amount of

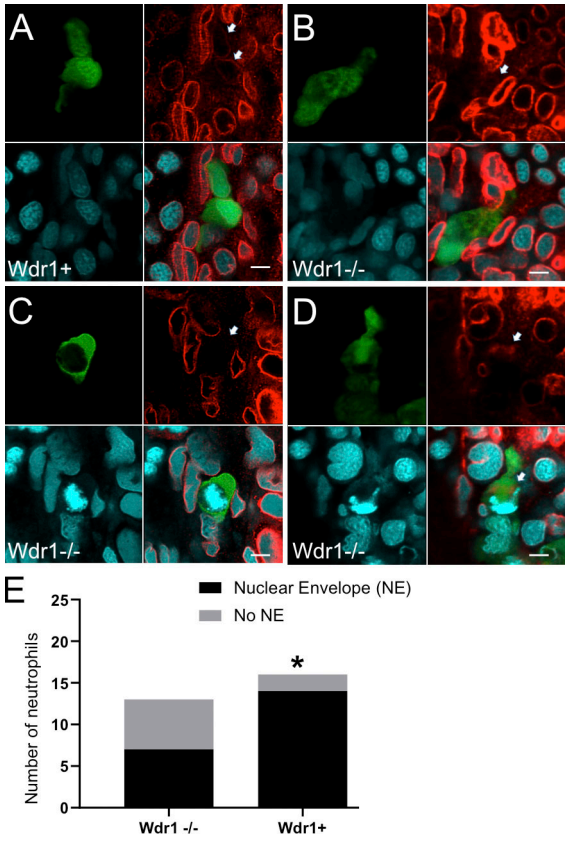


Figure 4. **Wdr1-deficient neutrophils lose their nuclear lamina. (A–E)** Whole-mount immunofluorescence images of neutrophils in sibling versus mutant Tg(Lyz:GFP) embryos at 2.5 dpf immunostained for Lamin B2 (red), with DNA stained by the far-red fluorescent dye RedDot 1 (cyan). Whereas lamin B2 delineated the nucleus in neutrophils of WT siblings (A, arrows), it did not in any late-stage mutant neutrophil (C and D) nor in some at early stage (B; see also Video 7). Aggregates of lamin B2 were often apparent instead (D, arrow). **(E)** Proportions of mutant ($n$ = 13) versus WT ($n$ = 16) neutrophils in which a full lamin B2–delineated NE was detected. $\chi^2$ test; *, $P < 0.05$. Scale bars, 5 µm.

pMLC in neutrophils (Fig. 5 E) and caused a neutrophil phenotype similar to Wdr1 deficiency, wherein nuclear dysmorphology was observed including chromatin unraveling, nuclear lamina disruption, and fragmentation/eruption of neutrophils (Fig. 5, F–J; and Video 8).

### Cofilin is constitutively active in Wdr1-deficient neutrophils

What could cause the uncoupling of myosin from F-actin in Wdr1-deficient neutrophils? An attractive candidate was cofilin, with which Wdr1 interacts to help sever and then fully depolymerize F-actin. Myosin and cofilin are indeed known competitors for binding to F-actin (Wiggan et al., 2012; Elam et al., 2013). Cofilin capacity to bind F-actin is tightly regulated by Ser3 phosphorylation: the phosphorylated form (hereafter designated as p-cofilin) is unable to bind F-actin. Therefore, we sought to compare the global amount, localization, and phosphorylation state of cofilin in mutant versus WT neutrophils via whole-mount immunohistochemistry, using antibodies against either all cofilin or p-cofilin.

Both immunostainings demonstrated marked differences between WT and mutant neutrophils. In WT neutrophils, cofilin was fairly evenly distributed throughout the cytoplasm with frequent enrichment at the cell cortex, which was also delineated by F-actin (Fig. 6 A), whereas in mutant neutrophils, cofilin accumulated into dense cytoplasmic areas that appeared to colocalize with the F-actin clumps (Fig. 6 B). The quantitative 3D image analysis revealed that even though the mutant neutrophils had on average one third less total cofilin than the WT (Fig. 6 C), they showed a clearly higher degree of colocalization of cofilin and F-actin, reflected in the Pearson as well as Manders' A and B coefficients (Fig. 6 D).

P-cofilin was detected in WT neutrophils throughout the cytoplasm (Fig. 6 E), whereas it was virtually unseen in mutant neutrophils (Fig. 6 F). The quantitative analysis confirmed that the mutant neutrophils contained fourfold less p-cofilin than the WT (Fig. 6 G). Interestingly, the analysis of p-cofilin/F-actin colocalization (Fig. 6 H) revealed a complete absence of spatial correlation in the WT neutrophils, with a mean Pearson coefficient close to zero, consistent with the reported inability of p-cofilin to bind F-actin.

Altogether, these data show that in mutant but not WT neutrophils, cofilin is mostly present in nonphosphorylated form, associated with F-actin. It is therefore expected to outcompete myosin for binding to F-actin, and this would lead to the observed spatial uncoupling of F-actin and pMLC. Moreover, the extensive coverage of actin filaments with cofilin in mutant neutrophils is expected to cause F-actin stabilization rather than severing (Jansen et al., 2015), especially in the absence of Wdr1, which facilitates F-actin severing by cofilin under high cofilin coverage of actin (Nadkarni and Brieher, 2014; see Discussion). This would lead to the defects in F-actin turnover that we have observed.

### Coronin 1A depletion fully rescues Wdr1-deficient neutrophils

Along with Wdr1, coronin 1 is known to influence the rate of F-actin severing by cofilin, either facilitating or hindering it, depending on the type of F-actin structure and other contextual parameters (Brieher et al., 2006; Cai et al., 2007; Galkin et al., 2008; Chan et al., 2011; Brieher, 2013). In addition, coronin 1B has been shown to induce cofilin dephosphorylation via recruitment of Slingshot phosphatase (Cai et al., 2007), so depleting coronin 1 might help normalize the cofilin phosphorylation level in wdr1$^{carmin}$ mutants. Coronin 1A is the main coronin in leukocytes. Therefore, we examined the effect of coronin 1A depletion in Wdr1-deficient *carmin* embryos, using antisense morpholinos to inhibit coronin 1A mRNA translation or splicing. Quite strikingly, whereas in WT sibling embryos coronin 1A depletion did not appear to affect neutrophil expansion or mobility, in *carmin* embryos it fully rescued neutrophils, restoring not only their numbers through time but also their actin dynamics, motility, and nuclear morphology (Figs. 7 and S4 and Video 8).

## Discussion

Recent studies have demonstrated a critical role of Wdr1 in the necessary breakdown and turnover of filamentous actin, as reviewed in Ono (2018). Moreover, its relevance to human disease has recently been pointed out by reports of *WDR1*-mutated patients that suffered immune deficiencies of two different types:

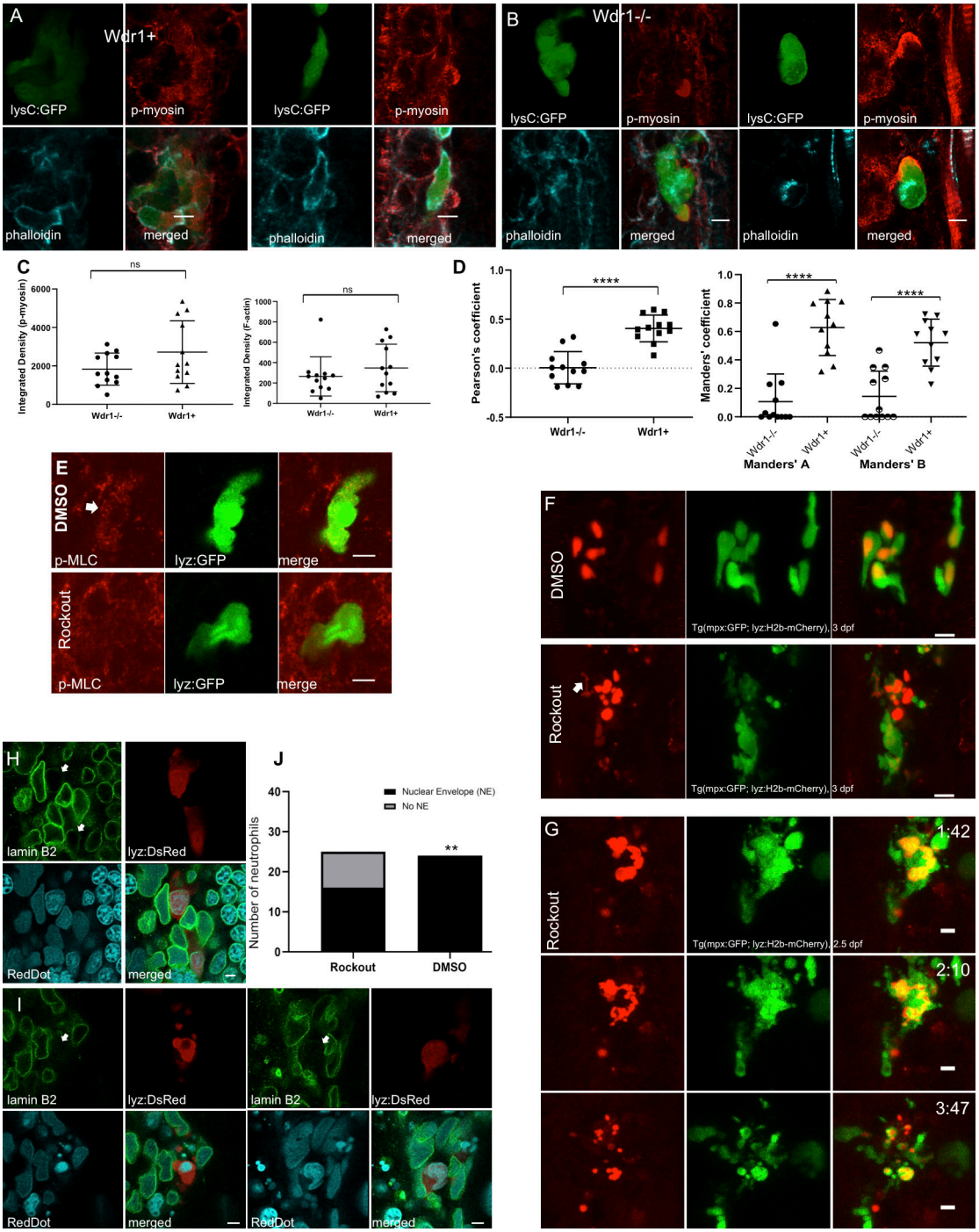


Figure 5. **Actomyosin perturbation plays a key role in the nuclear instability of Wdr1-deficient neutrophils. (A and B)** Whole-mount immunofluorescence confocal images of transgenic 2.5-dpf Tg(lyz:GFP) *carmin* mutant vand WT sibling probed with s19-pMLC antibody (red) and phalloidin (cyan). **(A)** In neutrophils of sibling embryos, pMLC appears both cortical (together with phalloidin-labeled F-actin) and diffusely cytoplasmic. **(B)** In mutants, intense caps of pMLC appear at the periphery of neutrophils, quite apart from their phalloidin-labeled cytoplasmic F-actin clumps. **(C and D)** Quantification of the mean intensity (C) and colocalization (D) of pMLC and F-actin in the 3D extent of individual mutant ($n$ = 12) versus WT sibling ($n$ = 12) neutrophils, all from the same experiment. For the Manders' coefficients, A is F-actin and B is pMLC. Data are mean ± SEM. For statistical analysis, Welch's $t$ test was used; ****, $P < 0.0001$. **(E–G)** WT Tg(mpx:GFP; lyz:H2b-mCherry) embryos were incubated in 200 µM Rockout at 2 dpf for 8–16 h. **(E)** Immunostaining confirmed decreased amounts of p-MLC upon Rockout treatment. **(F and G)** Live confocal imaging revealed within the neutrophils of Rockout treated embryos a reproduction of the characteristic chromatin (red) unwinding (F, arrow) and cell fragmentation (G) seen in neutrophils of Wdr1-deficient embryos. G shows selected time points of the time-lapse sequence shown in Video 8; time is indicated in h:min. **(H–J)** Immunostaining for Lamin B2 (red) in control (H, $n$ = 24) versus Rockout-treated embryos (I, $n$ = 25) demonstrated loss of NE in some neutrophils after Rockout treatment (I and J); all points are from the same experiment; for statistical analysis, a $\chi^2$ test was used; **, $P < 0.01$. Scale bars, 5 µm.

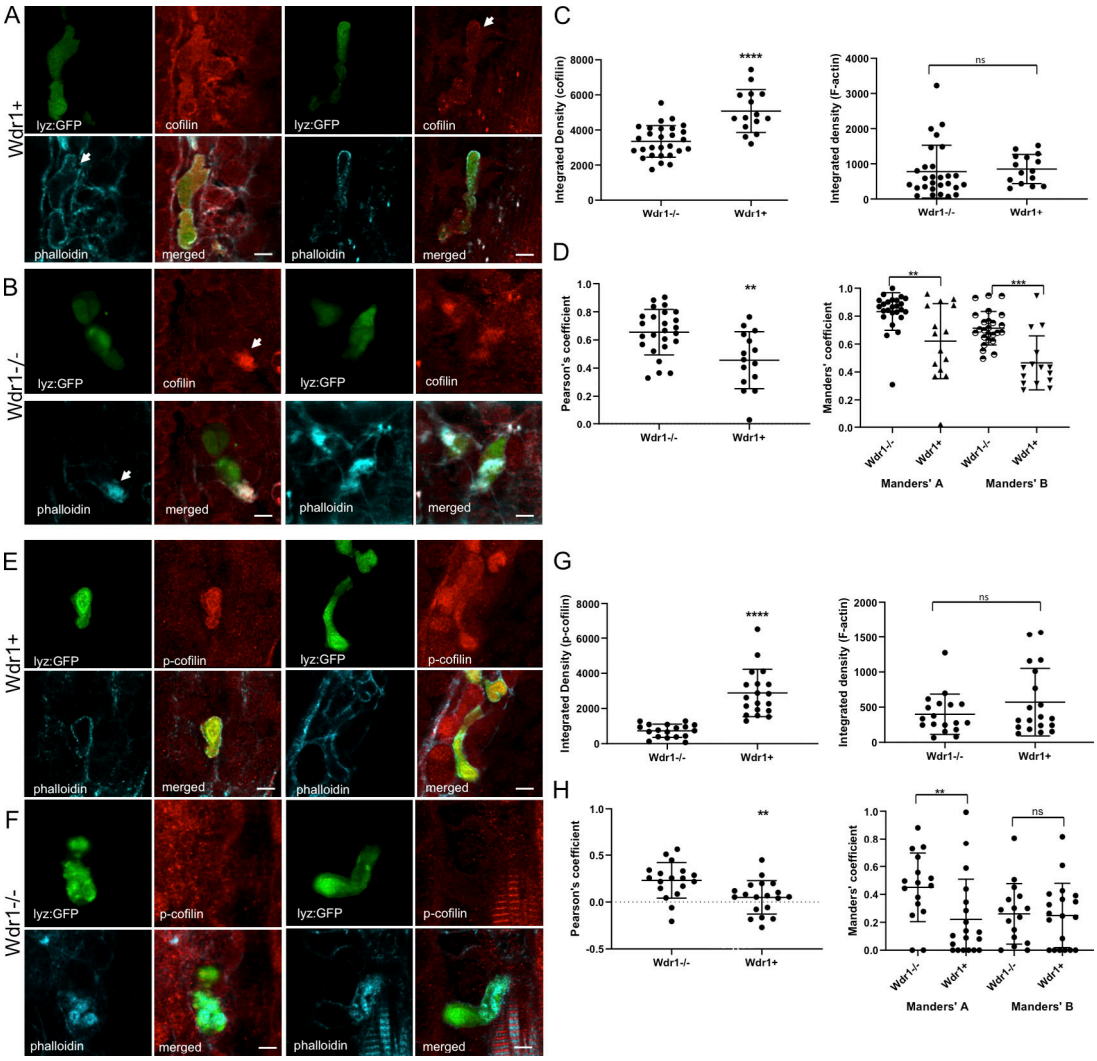


Figure 6. **Cofilin is constitutively active in Wdr1-deficient neutrophils. (A–H)** Whole-mount immunodetection in 2.5-dpf Tg(lyz:GFP) *carmin* and sibling embryos of whole cofilin (A–D) and Ser3-p-cofilin (E–H). **(A)** In neutrophils of WT sibling embryos, cofilin is detected throughout the cytoplasm with some enrichment at the cell cortex (arrow) clearly delineated by F-actin (cyan). **(B)** In mutant embryos, cofilin forms aggregates that correlate with the F-actin cytoplasmic clumps (arrows). **(C and D)** Quantitative analysis of the mean density (C) and colocalization (D) of pMLC and F-actin in the 3D extent of individual mutant ($n$ = 25) versus WT sibling ($n$ = 15) neutrophils, all from the same experiment. For the Manders' coefficients, A is F-actin and B is cofilin. **(E and F)** In the neutrophils of sibling embryos (E), p-cofilin was readily detected as a diffuse signal throughout the cell, whereas in the neutrophils of mutant embryos (F), p-cofilin was not visible. **(G and H)** Quantitative analysis of the mean density (G) and colocalization (H) of p-cofilin and F-actin in the 3D extent of individual mutant ($n$ = 18) versus WT sibling ($n$ = 19) neutrophils, all from the same experiment. For the Manders' coefficients, A is F-actin and B is p-cofilin. In all graphs, data are mean ± SEM; for statistical analysis, Welch's $t$ test was used. ns, nonsignificant ($P > 0.05$); **, $P < 0.01$; ***, $P < 0.001$; ****, $P < 0.0001$. Scale bars, 5 µm.

(1) an autoinflammatory syndrome including neutrophilia, WDR1 intracellular aggregates, and IL18 production (one family/one mutation; Standing et al., 2017), and (2) LLS, characterized by recurrent infections due to the defective mobilization of neutrophils to inflammatory stimuli (six families/eight mutations; Kuhns et al., 2016; Pfajfer et al., 2018). The phenotype of our wdr1$^{carmin}$ mutant zebrafish diverges from the autoinflammatory syndrome, showing no increase in assessed inflammatory cytokines (not depicted), but is close to the LLS. Two typical traits of LLS are excess F-actin in neutrophils, manifesting as F-actin clumps throughout the cytoplasm instead of the normal, mostly cortical localization (Foroozanfar et al., 1984; Goldman et al., 1984), and the herniation of their nuclei (Kuhns et al., 2016). The recent identification of *WDR1* missense mutations in LLS patients from six different families suggests that WDR1 deficiency could be the cause of most if not all LLS cases. The similar phenotype of neutrophils in our Wdr1-deficient zebrafish reinforces that prospect.

Although in our wdr1$^{carmin}$ mutant, neutrophils are the first cell type to be visibly affected during fish development, over the next days the maturation of epithelia and muscles becomes increasingly affected, leading to larval death. In line with this, whole-animal *Wdr1* knockout is lethal in mice (at embryonic peri-implantation stage), and Wdr1 was found to be important for epithelial polarity and for sarcomeric actin assembly in striated and cardiac muscles (Yuan et al., 2014; Ono, 2018).

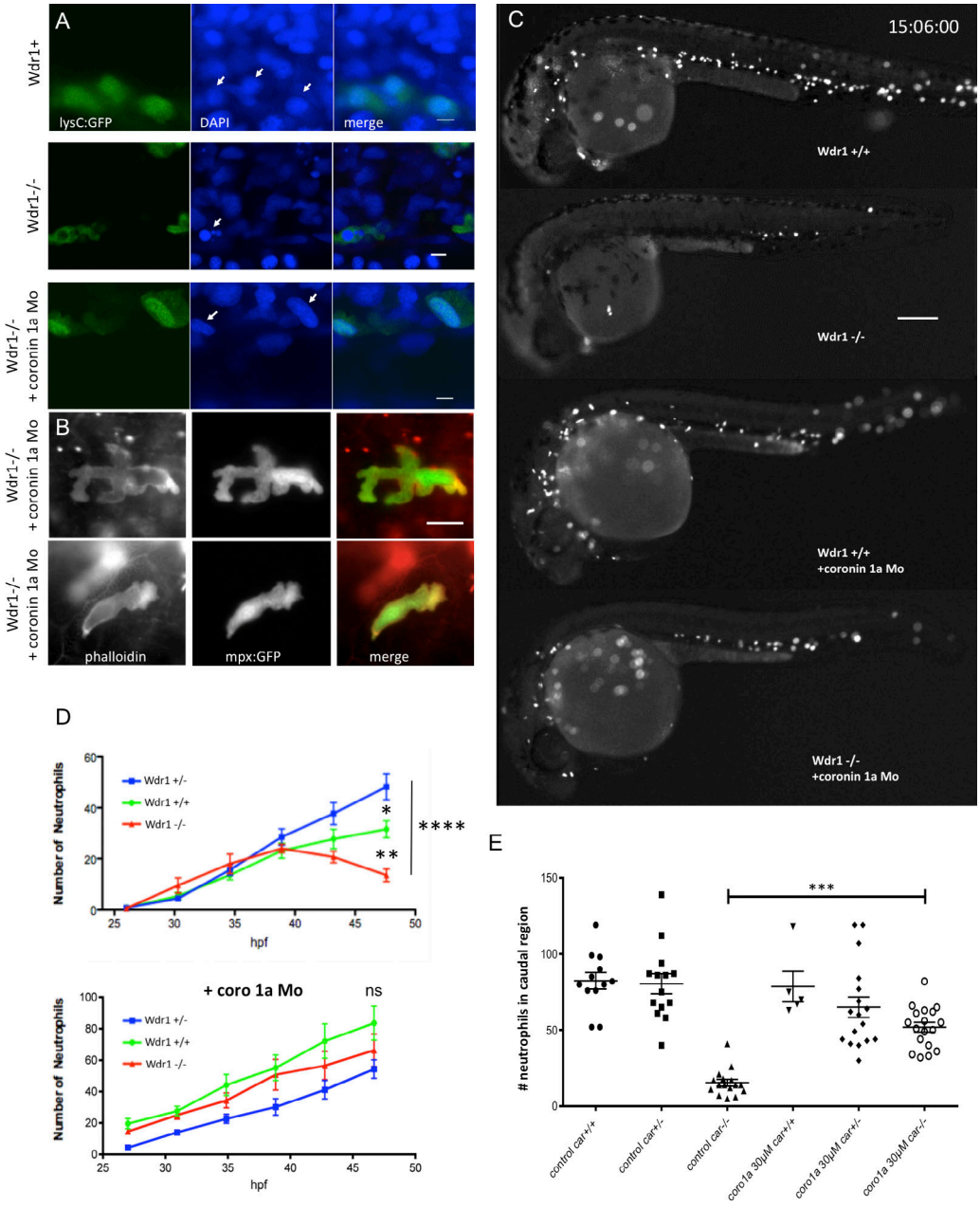


Figure 7. **Coronin 1A depletion fully rescues Wdr1-deficient neutrophils. (A)** Images of 2.5-dpf whole-mount DAPI-stained Tg(lyz:GFP) Wdr1$^{+}$, Wdr1$^{-/-}$, and Wdr1$^{-/-}$ embryos injected with a coronin 1A translation-blocking morpholino. Coronin 1A knockdown has restored the nuclear integrity of mutant neutrophils compared with the fractionated nuclei of untreated embryos (arrows). **(B)** Phalloidin staining of neutrophils in coro1a morpholino–injected Wdr1$^{-/-}$ embryos shows that their typical shape and cortical location of F-actin has been restored; the nucleus also remains GFP enriched. **(C and D)** Control or morpholino-injected *carmin* and sibling embryos were mounted in agarose by 26 hpf, time-lapse imaged in parallel for 20–24 h via a wide-field microscope, and later genotyped. **(C)** Representative images of sibling, mutant, and coro1a-ATG Mo–injected mutant embryos after 15 h of time-lapse imaging (see also Video 8). **(D)** Neutrophil counts over time in embryos of the three genotypes, either uninjected (upper graph, $n$ = 39) or injected with the coro1a-ATG morpholino (lower graph, $n$ = 40), as derived from the time-lapse videos. All points are from the same experiment. Data are mean ± SEM. *, P < 0.05; **, P < 0.01; ****, P < 0.0001 with two-tailed unpaired $t$ test. **(E)** Neutrophil counts at 56 hpf in the caudal half of embryos injected with control ($n$ = 42) or coro1a-ATG morpholino ($n$ = 40) and later genotyped. All points are from the same experiment. Data are mean ± SEM. Statistical significance was determined by one-way ANOVA, with Tukey's multiple comparisons test. ***, P ≤ 0.001. Differences between injected WT and rescued mutant embryos are statistically nonsignificant (P > 0.05). Scale bars, 5 µm (A), 10 µm (B), and 100 µm (C).

In contrast, it seems that beyond their high rates of infection due to crippled neutrophils, LLS patients developed normally and can live a normal life. In light of our results, we conclude (a) that their WDR1 mutations are probably hypomorphic, unlike the *carmin* mutation, and (b) that the neutrophil is the cell type most sensitive to Wdr1 dysfunction, in both mammals and zebrafish.

Given the role of Wdr1/Aip1 in F-actin depolymerization, it is not unexpected that its malfunction first affects the highly

mobile neutrophils, as their ameboid motility requires a high level of F-actin turnover. More enigmatic was the typical herniation of the neutrophil nucleus, seen in both LLS and the autoinflammatory syndrome. In the zebrafish embryo, thanks to high-magnification in vivo time-lapse imaging, we could see the nuclear herniations develop into a striking unwinding of the nuclear material that lasted for hours before the cell's demise, a phenomenon so far never reported in any cell type, to our knowledge. We found that this nuclear phenotype is accompanied by a loss of the nuclear lamina, as visualized by lamin B2 immunostaining, that seems to occur early in the unwinding process, and is bound to cause NE rupture.

Situations of transient NE rupture and associated nuclear herniations have recently been described in adherent cells, migratory cancer cells, and dendritic cells migrating through constricted spaces and were always found to occur at the site of gaps in the nuclear lamina (Denais et al., 2016; Hatch and Hetzer, 2016; Lammerding and Wolf, 2016; Raab et al., 2016; Thiam et al., 2016; Hatch, 2018). In all cases, NE rupture was found to originate in mechanical stress due to, for example, actin stress cables compressing the nucleus or to excess actomyosin contractility (Denais et al., 2016; Hatch and Hetzer, 2016; Lammerding and Wolf, 2016; Hatch, 2018), in which case the LINC (linker of nucleoskeleton and cytoskeleton) complex (that links cytoplasmic F-actin to the nuclear lamina, in a lamin A-dependent way) was often also involved (Khatau et al., 2010; Kim et al., 2017).

However, all these studies dealt with transient and/or local NE ruptures and associated nuclear lamina discontinuities, far from the irreversible nuclear lamina dissolution that we witnessed in Wdr1-deficient neutrophils. We think that this extreme phenotype may originate in the special nature of the NE in neutrophils. Mammalian as well as zebrafish neutrophils essentially lack lamin A, have low levels of B-lamins, and lack nesprins, the main component of the LINC complex (Olins et al., 2008, 2009; Singh et al., 2013a). The lamin A level specifies the rigidity of the NE; its absence in neutrophils leads to a highly flexible nucleus, which allows them to migrate through smaller pores than any other cell type (Rowat et al., 2013). The downside of lamin A absence is thought to be a more fragile nucleus (Olins et al., 2009; Harada et al., 2014); however, this consequence was shown only upon lamin A depletion or mutation in cells that normally express it. The neutrophil nucleus might obey a different logic, whereby its high deformability might actually make it less prone to mechanical stress–induced NE breaks. In the unusual case of the LINC-less neutrophil (where LINC is thought to be essential for force transmission from the cytoskeleton to the nucleus), the nature of the connection between the nucleus and cytoskeleton remains to be explored. Our data provide a first hint, as we found that in contrast with all cases cited above, where excessive actomyosin contractility favored or triggered NE rupture, actomyosin contractility was necessary to maintain the integrity of the NE of neutrophils in WT zebrafish embryos. We surmise that this also holds for mammalian neutrophils, based on the nuclear phenotype of LLS neutrophils.

Given such a role of actomyosin contractility in neutrophil NE maintenance, our finding that in *carmin* neutrophils pMLC becomes completely spatially uncoupled from F-actin predicts the observed breakdown of their NE. This spatial uncoupling of F-actin and pMLC in Wdr1-deficient neutrophils is likely due to the exclusion of myosin from F-actin by competing cofilin (Kuhn and Bamburg, 2008; Wiggan et al., 2012; Elam et al., 2013). Two phenomena indeed support this hypothesis. First, in the Wdr1-deficient neutrophils, unlike in WT, we found cofilin to be mostly in its unphosphorylated, active form (i.e., able to bind F-actin), and consequently most if not all cofilin would be bound to F-actin. This overall dephosphorylation of cofilin was also found in *Wdr1* knockout mouse cells (Xiao et al., 2017) and in the neutrophils of an LLS patient harboring a D26N mutation in Wdr1 (Kuhns et al., 2016). Xiao et al. (2017) were able to explain this effect of Wdr1 deficiency by showing that mouse WDR1 binds to the LIM-kinase (LIMK1) microtubule binding domain, thus preventing its inhibitory localization to microtubules and enhancing its ability to phosphorylate cofilin. Interestingly, even though the two point mutations shown to cause cofilin unphosphorylation, our carmin W540R and the human D26N. lie far apart on the Wdr1 primary sequence, in the 3D crystal structure they both lie near the convex surface of the protein, opposite to the concave surface where cofilin is thought to bind (Ono, 2018). This would suggest that it is the convex side of the Wdr1 protein that binds the PDZ domain of Lim kinase, thus promoting the phosphorylation of cofilin bound to the other, concave side of Wdr1.

Second, and particularly in the presence of the highly abundant coronin 1A, which helps cofilin to bind cooperatively to F-actin, Wdr1 deficiency is predicted to favor a full coverage of F-actin by cofilin, for in the absence of Wdr1, cofilin-covered actin filaments are stable (Elam et al., 2013; Gressin et al., 2015; Jansen et al., 2015). The sum of these effects would lead, upon Wdr1 deficiency, to an excess of stable actin filaments, possibly all covered by cofilin and coronin.

We found that the adverse effects of Wdr1 deficiency on zebrafish neutrophils can be fully rescued by knocking down expression of their main coronin, coronin 1A. This effect may seem paradoxical at first, since coronins and Wdr1 are both thought to help cofilin sever F-actin. Yet we envision two ways in which coronin 1A depletion could counteract the adverse effects of Wdr1 deficiency.

First, while the three factors together are considered to be the optimal combination for F-actin severing, recent data (Jansen et al., 2015) indicate that coronin binds to F-actin first and enhances subsequent cofilin binding, and maximal severing occurs after Wdr1 also binds. In the absence of both Wdr1 and coronin, actin filaments are thus predicted to be less saturated with cofilin, thereby bringing the latter's density closer to optimal for F-actin severing without Aip1/Wdr1 help (Fig. 8). In addition, coronin 1A has been found to stabilize actin filaments by stapling them together (Galkin et al., 2008), and that effect would be suppressed upon coronin 1A depletion.

Second, coronin 1B has been shown to interact with and activate Slingshot phosphatase, thus promoting cofilin dephosphorylation (Cai et al., 2007). That property may be shared by coronin 1A, for its depletion in COS cells has been observed to increase levels of p-cofilin, and interestingly, also of pMLC and cell contractility (Ojeda et al., 2014). Still, given the delicate, fine

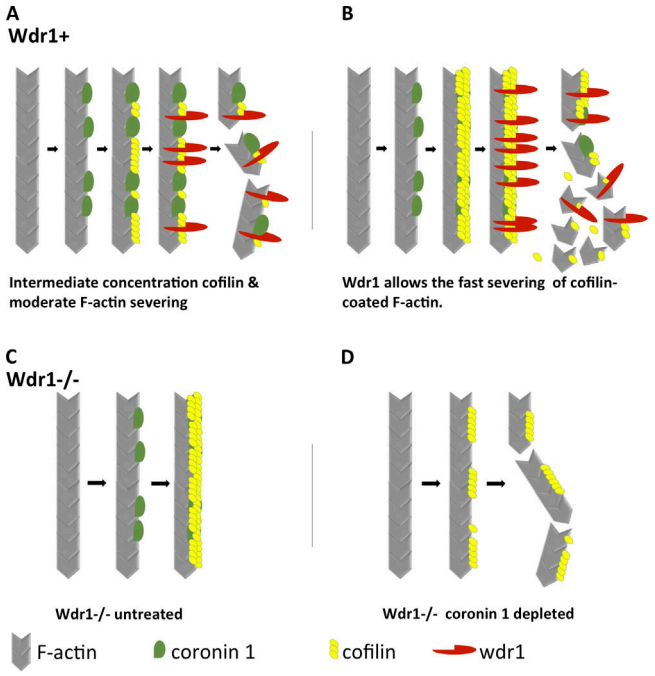


Figure 8. **A model of F-actin severing in Wdr1-deficient versus Wdr1-proficient neutrophils and rescue of the former by coronin 1A depletion.** **(A)** Coronin 1 binding increases recruitment of cofilin, which in turn recruits Wdr1 (Jansen et al., 2015). When cofilin is present in intermediate concentrations, it moderately severs actin filaments at transition sites between cofilin-bound and -bare F-actin, without potentiation by Wdr1. **(B)** In high cofilin concentration conditions, cofilin instead stabilizes actin filaments. However, Wdr1 binding to the cofilin-bound actin filaments triggers fast severing of the filaments (Ono, 2018). **(C)** In Wdr1-deficient neutrophils, coronin 1A binds actin filaments and recruits cofilin. In the absence of Wdr1, cofilin is fully unphosphorylated and thus fully coats and stabilizes F-actin. **(D)** When Wdr1-deficient embryos are depleted of coronin 1A, the absence of coronin 1A on F-actin lowers the binding of cofilin. Moderate concentrations of bound cofilin, despite the absence of Wdr1, can now sever actin at moderate rates.

tuning of the actin dynamics pathways involved in leukocyte cell migration, it is striking to witness that not only did coronin 1A depletion rescue neutrophils from death, but also their full amoeboid motility was restored. This result will be an important piece of data to consider for any future modeling of leukocyte ameboid motility in vivo. Meanwhile, the complete restoration of Wdr1-deficient neutrophils by coronin 1A depletion may open a new prospect for the treatment of LLS patients. Moreover, since the *WDR1* mutations found in LLS patients are presumably hypomorphic relative to the *carmin* mutation, an even milder manipulation of coronin 1A expression or activity might well suffice to correct the disease.

## Materials and methods

### Zebrafish lines and maintenance

WT AB and transgenic stocks of zebrafish were maintained as described previously (Westerfield, 2000). Embryos were maintained in 0.003% 1-phenyl-2-thiourea to inhibit pigmentation, for maximum transparency, and anesthetized with 0.016% (wt/vol) Tricaine before experimental manipulation. The following transgenic lines were used: Tg(mpx:GFP)$^{i114}$ (Renshaw et al., 2006), Tg(lyz:EGFP)$^{nz117}$ and Tg(lyz:DsRed2)$^{nz50}$ (Hall et al., 2012), and Tg(lyz:H2b-mCherry)$^{ump8}$ (G. Lutfalla, Centre National de la Recherche Scientifique/University of Montpellier, Montpellier, France). Their details can be accessed on the Zebrafish Information Network database (http://zfin.org) via their above allele names.

### Generation and identification of the *carmin* mutant

The *carmin* mutant was identified in a large-scale *N*-ethyl-*N*-nitrosourea mutagenesis screen (ZF-Models Consortium mutagenesis screen [http://zfin.org/ZDB-PUB-060606-1]) wherein Sudan black staining (Le Guyader et al., 2008) was used to screen for neutropenic mutants. Meiotic mapping of *carmin* was performed using standard simple sequence length polymorphisms. The *carmin* gene was PCR amplified from cDNA made from mutant and WT siblings (primers: forward 5′-TTCAGCTCCGTTCAGCCGTTATTC-3′ and reverse 5′-ACGCTG AGCTCTGCTTCTGGAATG-3′). The amplicons were then further amplified using nested primers (forward 5′-TACCGGAGG AGAACACGCAGACAT-3′, reverse 5′-TGAGGAGGAGAGTGG AACATCAGA-3′, and reverse 5′-TCTGAGCTGTTGAGGAGG AGAGTG-3′). Amplified DNA was then purified by polyethylene glycol precipitation and sequenced (primers: 5′-TACCGG AGGAGAACACGCAGACAT-3′, 5′-TGAGGAGGAGAGTGGAAC ATCAGA-3′, 5′-CAATCTCCCCCACTGAAGAA-3′, and 5′-AGA AGGTGGTCACGGTGTTC-3′). Genomic exon sequencing was performed by amplifying Wdr1 exon 11 (5′-AGCGAGTTCTAC GGGCATC-3′, 5′-TGGCAGCTTGATCCTCTTCT-3′, 5′-AGTGAG TTCTACGGGCATC-3′, and 5′-CGGCAGCTTGATCCTCTTCT-3′) and cloning the fragments into a Topo TA vector.

### Genotyping

Melting-curve genotyping was performed as previously described (Palais et al., 2005), wherein PCR primers were designed bracketing the *carmin* mutation: (5′-CGAAGGTGGTGTGTCTGT CC-3′ and reverse 5′-TGGTGGCGAAGTGCTCATTA-3′). Melting curves were generated either with an Idaho technology plate reader or in a PCR machine.

### Confocal fluorescence imaging

Zebrafish embryos were anesthetized with 0.02% Tricaine and embedded in 1% low-melting-point agarose/volvic $H_2O$ in glass-bottom µ-dishes at RT. Images were captured using Leica SP8 inverted and SPE inverted and upright confocal microscopy setups; the objectives used were HC PL APO CS2 20×/0.75 and 40×/1.10 water-immersion objectives on the SP8 setup, PL Fluotar 16×/0.50 and ACS APO 40×/1.15 oil-immersion objectives on the SPE inverted setup, and a HCX APO L U-V-I 20×/0.50 water-immersion objective on the SPE upright setup. To generate images of whole embryos, a mosaic of (512 × 512-pixel) confocal z-stacks of images taken with the 20× objective of the SP8 setup was stitched together using the Mosaic Merge function of the LASx software.

### Pharmacological inhibition of Rho-Rock signaling

2-dpf and 2.5-dpf embryos were dechorionated and placed in 100–200 µM Rockout (Rho kinase inhibitor III) or control

DMSO/Volvic water, in 6-well plates and kept at RT. At intervals of 8, 12, 16, and 24 h after incubation, they were mounted in 1% low-melting-point agarose (supplemented with Tricaine/$H_2O$ with or without Rockout) and imaged via the Leica SP8 confocal microscopy setup.

### Morpholino and plasmid injections

Morpholino oligonucleotides (Gene Tools) were injected into 1–2–cell stage embryos (1.2 nl/embryo) at the concentration indicated in the figures. We used two splice-blocking morpholinos against the wdr1 gene: wdr1 E3 (5′-ACTCACACTCACTCACCGCCC GATG-3′) and wdr1 E4 (5′-GTCCAGCAGCGGTCACTCACTTCTC-3′), two morpholinos to target the coro1a gene, a translation-blocking morpholino, coro1a ATG (5′-ACCTTCCTAGACATGATG ACCTGAG-3′), a splice-blocking morpholino, coro1a xi3 (5′-ATG AAGTCCTTGTCACTCACCATGA-3′), and a standard control morpholino (5′-CCTCTTACCTCAGTTACAATTTATA-3′).

For transient expression in developing embryos, plasmids containing mpx:Lifeact-Ruby or lyz:H2b-mCherry transcription units and Tol2 transposition sites (Yoo et al., 2010, 2012) were coinjected with Tol2 transposase mRNA into Tg(mpx:GFP) embryos at the 1-cell stage (2.5–5 pg/embryo).

### Whole-mount immunohistochemistry and TUNEL staining

We used rabbit anti-phospho(ser19)-myosin light chain antibody (1:25, 3671S; Cell Signaling); mouse anti-lamin B2 (1:25, ab8983 Abcam); rabbit and mouse anti-cofilin (1:25, SAB4300577, SAB2702206), rabbit anti-phospho(ser3)-cofilin (1:25, SAB4300115) from Sigma-Aldrich, and phalloidin Alexa Fluor 647 or Alexa Fluor 488 (1:10, A22287 and A12379; Molecular Probes). The secondary antibodies (used at 1:300) were Alexa Fluor 488–conjugated goat anti-mouse (Thermo Fisher Scientific; A11017), Cy3-conjugated goat anti-mouse and anti-rabbit (Jackson Immunoresearch; 115-166-003 and 111–166-003). Whole embryos were fixed in 4% formaldehyde/microtubule stabilizing buffer for either 2–4 h at RT or overnight at 4°C, and then quenched with $NaBH_4$/PBS as described previously (McMenamin et al., 2003). After washes in PBSDT (PBS, 1% DMSO, and 0.1% Tween), they were treated with $H_2O$/0.1% Tween for 30 min at RT and acetone at −20° for 20 min, rinsed with 1× HBSS/0.1% Tween, permeabilized with collagenase solution (Svoboda et al., 2001) for up to 1.5 h, washed, blocked with 10% Western blocking solution/PBSDT, and then incubated for 24–48 h at 4°C with the primary antibodies. Following washes, embryos were blocked in 10% Western blocking solution/PBSDT again before 24–48-h incubation in secondary antibodies at 4°C with agitation. After multiple washes, Hoechst 33342 (2 µg/ml) or RedDot 1 (1:200, BTM40060-T; Biotium) was applied for 30–60 min at RT, and the embryos were washed again in PBSDT. They were then either embedded in 1% low-melting-point agarose/$H_2O$ or mixed 1:1 with Mowiol 4-88 (Fluka; 8138) in glass-bottom µ-dishes for confocal imaging.

The specificity of the anti-cofilin and anti-p-cofilin antibodies in the zebrafish embryos was confirmed by the following observations: the p-cofilin and whole-cofilin antibodies both labeled periodic striations in somite muscles intercalated with phalloidin/pMLC-labeled striations. In addition, the whole-cofilin, but not the p-cofilin, antibodies delineated periderm cell contours (as does phalloidin), and quite strongly the characteristic F-actin microridges at the surface of these cells, indicating that in these structures, cofilin is in the non-phosphorylated (hence potentially actin-binding) form, consistent with the fact that these actin microridges were shown to be dynamic (Lam et al., 2015). TUNEL staining was performed using the Apoptag Red In situ Apoptosis Detection Kit (Merck Millipore).

### Image analysis and statistics

For quantifying neutrophil numbers in live embryos as in Fig. 1 B, lyz:GFP$^+$ neutrophils were manually counted on maximum-projection images from mosaic confocal z-stacks of whole embryos obtained by stitching tile scans obtained with the 20× objective.

For the quantitative analysis of immunohistochemically stained embryos, confocal image z-stacks acquired and then deconvoluted via the Lightning deconvolution system implemented in LASx software driving the Leica SP8 setup were then analyzed with Imaris software (Bitplane). Individual neutrophils were segmented in 3D from their histological environment based on their GFP content, and their content in phalloidin/F-actin, cofilin, p-cofilin, and pMLC was quantified via the 3DView module. The colocalization of F-actin with the immunolabeled molecule was then analyzed within each segmented neutrophil via the Colocalization module. The Pearson correlation coefficient was calculated first; if it was >0, the Costes thresholds and the Manders' A and B coefficients were calculated (Manders' A = fraction of F-actin colocalizing with immunolabeled molecule intensity above the Costes threshold calculated for the latter, and vice versa for Manders' B). GraphPad Prism was used for statistical analysis of all the data, using the tests indicated in the figure legends.

### Online supplemental material

Fig. S1 (related to Fig. 1) shows that a retroviral insertion wdr1 mutant does not complement the carmin mutant for the loss of neutrophils, confirming that the wdr1 mutation in *carmin* is the causative mutation. Fig. S2 (related to Fig. 2) shows the overall phenotype of the mutant beyond the loss of neutrophils. Fig. S3 (related to Fig. 3) shows that like their WT siblings, neutrophils of *carmin* mutants have one and only one centrosome. Fig. S4 (related to Fig. 7) shows that both a splice-blocking and a translation-blocking morpholino rescue neutrophils in Wdr1-deficient embryos. Video 1 (related to Fig. 1) shows by time-lapse confocal imaging the gradual decrease and reduced mobility of neutrophils in a whole *carmin* embryo compared with a WT sibling. Video 2 (related to Fig. 2) shows by time-lapse confocal imaging of embryos expressing Lifeact-Ruby in neutrophils the intense F-actin clumps and reduced mobility of neutrophils in a carmin embryo compared with a WT sibling. Video 3 (related to Fig. 3) is confocal z-stack through a mutant neutrophil illustrating that their nucleus becomes multiglobular. Video 4 (related to Fig. 3) shows by in vivo time-lapse confocal imaging in mutant and WT sibling embryos of neutrophils expressing H2b-mCherry the unusual nuclear/chromatin fluidity

or unwinding in mutant neutrophils, followed by their eruption. Video 5 then shows in more detail the successive stages of chromatin lengthy unwinding, then rapid condensation, followed by cell fragmentation. Video 6 then shows that macrophages in the vicinity of neutrophils engulf neutrophils only once they have reached the stage of chromatin condensation. Video 7 (related to Fig. 4) shows through a confocal z-stack three mutant neutrophils with still uncondensed nucleus/chromatin that display no lamin B2 stained NE. Video 8 (related to Fig. 5) shows via time-lapse confocal imaging of a Rockout-treated WT embryo that neutrophils undergo a pathology similar to that seen in *carmin* embryos. Video 9 (related to Fig. 7) shows by time-lapse imaging that coronin 1A knockdown fully rescues neutrophils in *carmin* embryos.

## Acknowledgments

We are grateful to A. Huttenlocher and P. Lam (University of Wisconsin, Madison, WI) for mpx:Lifeact-Ruby and lyz:H2b-mCherry encoding plasmids, G. Lutfalla for Tg(lyz:H2b-mCherry)$^{ump8}$ transgenic zebrafish, N. Trede for supporting M. Redd in the molecular elucidation of the carmin causative mutation, E. Sahai for sharing unpublished data from his laboratory, and J-Y. Tinevez for guidance in image analysis software.

This work was supported by an E-Rare grant from the European Union (Neutro-Net) and by Equipe Fondation Recherche Médicale grants from the Fondation pour la Recherche Médicale (DEQ20120323714 and DEQ20160334881) to P. Herbomel.

The authors declare no competing financial interests.

Author contributions: M. Redd and P. Herbomel conceived the project. E. Murayama isolated the *carmin* mutant, and M. Tauzin conceived and performed its initial phenotypic characterization. M. Redd, M. Yousfi, and C. Bowes conceived, performed, and analyzed the results of most experiments. C. Bowes and P. Herbomel wrote the manuscript. P. Herbomel analyzed the data, supervised the project, and obtained funding.

Submitted: 6 January 2019
Revised: 20 June 2019
Accepted: 1 August 2019

## References

Amsterdam, A., R.M. Nissen, Z. Sun, E.C. Swindell, S. Farrington, and N. Hopkins. 2004. Identification of 315 genes essential for early zebrafish development. *Proc. Natl. Acad. Sci. USA.* 101:12792–12797. https://doi.org/10.1073/pnas.0403929101

Andrianantoandro, E., and T.D. Pollard. 2006. Mechanism of actin filament turnover by severing and nucleation at different concentrations of ADF/cofilin. *Mol. Cell.* 24:13–23. https://doi.org/10.1016/j.molcel.2006.08.006

Bamburg, J.R., A. McGough, and S. Ono. 1999. Putting a new twist on actin: ADF/cofilins modulate actin dynamics. *Trends Cell Biol.* 9:364–370. https://doi.org/10.1016/S0962-8924(99)01619-0

Blanchoin, L., R. Boujemaa-Paterski, C. Sykes, and J. Plastino. 2014. Actin dynamics, architecture, and mechanics in cell motility. *Physiol. Rev.* 94:235–263. https://doi.org/10.1152/physrev.00018.2013

Brieher, W. 2013. Mechanisms of actin disassembly. *Mol. Biol. Cell.* 24:2299–2302. https://doi.org/10.1091/mbc.e12-09-0694

Brieher, W.M., H.Y. Kueh, B.A. Ballif, and T.J. Mitchison. 2006. Rapid actin monomer-insensitive depolymerization of Listeria actin comet tails by cofilin, coronin, and Aip1. *J. Cell Biol.* 175:315–324. https://doi.org/10.1083/jcb.200603149

Cai, L., T.W. Marshall, A.C. Uetrecht, D.A. Schafer, and J.E. Bear. 2007. Coronin 1B coordinates Arp2/3 complex and cofilin activities at the leading edge. *Cell.* 128:915–929. https://doi.org/10.1016/j.cell.2007.01.031

Chan, K.T., S.J. Creed, and J.E. Bear. 2011. Unraveling the enigma: progress towards understanding the coronin family of actin regulators. *Trends Cell Biol.* 21:481–488. https://doi.org/10.1016/j.tcb.2011.04.004

Denais, C.M., R.M. Gilbert, P. Isermann, A.L. McGregor, M. te Lindert, B. Weigelin, P.M. Davidson, P. Friedl, K. Wolf, and J. Lammerding. 2016. Nuclear envelope rupture and repair during cancer cell migration. *Science.* 352:353–358. https://doi.org/10.1126/science.aad7297

Elam, W.A., H. Kang, and E.M. De La Cruz. 2013. Competitive displacement of cofilin can promote actin filament severing. *Biochem. Biophys. Res. Commun.* 438:728–731. https://doi.org/10.1016/j.bbrc.2013.07.109

Fagerberg, L., B.M. Hallström, P. Oksvold, C. Kampf, D. Djureinovic, J. Odeberg, M. Habuka, S. Tahmasebpoor, A. Danielsson, K. Edlund, et al. 2014. Analysis of the human tissue-specific expression by genome-wide integration of transcriptomics and antibody-based proteomics. *Mol. Cell. Proteomics.* 13:397–406. https://doi.org/10.1074/mcp.M113.035600

Foroozanfar, N., P.H. Grohmann, and J.R. Hobbs. 1984. Abnormal fluorescent actin pattern of lazy phagocyte syndromes. *Diagn. Immunol.* 2:25–29.

Fox, S., A.E. Leitch, R. Duffin, C. Haslett, and A.G. Rossi. 2010. Neutrophil apoptosis: relevance to the innate immune response and inflammatory disease. *J. Innate Immun.* 2:216–227. https://doi.org/10.1159/000284367

Galkin, V.E., A. Orlova, N. Lukoyanova, W. Wriggers, and E.H. Egelman. 2001. Actin depolymerizing factor stabilizes an existing state of F-actin and can change the tilt of F-actin subunits. *J. Cell Biol.* 153:75–86. https://doi.org/10.1083/jcb.153.1.75

Galkin, V.E., A. Orlova, W. Brieher, H.Y. Kueh, T.J. Mitchison, and E.H. Egelman. 2008. Coronin-1A stabilizes F-actin by bridging adjacent actin protomers and stapling opposite strands of the actin filament. *J. Mol. Biol.* 376:607–613. https://doi.org/10.1016/j.jmb.2007.12.007

Gandhi, M., and B.L. Goode. 2008. Coronin: the double-edged sword of actin dynamics. *Subcell. Biochem.* 48:72–87. https://doi.org/10.1007/978-0-387-09595-0_7

Goldman, J.M., N. Foroozanfar, B.G. Gazzard, and J.R. Hobbs. 1984. Lazy leukocyte syndrome. *J. R. Soc. Med.* 77:140–141. https://doi.org/10.1177/014107688407700216

Gressin, L., A. Guillotin, C. Guérin, L. Blanchoin, and A. Michelot. 2015. Architecture dependence of actin filament network disassembly. *Curr. Biol.* 25:1437–1447. https://doi.org/10.1016/j.cub.2015.04.011

Hall, C.J., M.V. Flores, S.H. Oehlers, L.E. Sanderson, E.Y. Lam, K.E. Crosier, and P.S. Crosier. 2012. Infection-responsive expansion of the hematopoietic stem and progenitor cell compartment in zebrafish is dependent upon inducible nitric oxide. *Cell Stem Cell.* 10:198–209. https://doi.org/10.1016/j.stem.2012.01.007

Harada, T., J. Swift, J. Irianto, J.-W. Shin, K.R. Spinler, A. Athirasala, R. Diegmiller, P.C.D.P. Dingal, I.L. Ivanovska, and D.E. Discher. 2014. Nuclear lamin stiffness is a barrier to 3D migration, but softness can limit survival. *J. Cell Biol.* 204:669–682. https://doi.org/10.1083/jcb.201308029

Hatch, E.M. 2018. Nuclear envelope rupture: little holes, big openings. *Curr. Opin. Cell Biol.* 52:66–72. https://doi.org/10.1016/j.ceb.2018.02.001

Hatch, E.M., and M.W. Hetzer. 2016. Nuclear envelope rupture is induced by actin-based nucleus confinement. *J. Cell Biol.* 215:27–36. https://doi.org/10.1083/jcb.201603053

Jansen, S., A. Collins, S.M. Chin, C.A. Ydenberg, J. Gelles, and B.L. Goode. 2015. Single-molecule imaging of a three-component ordered actin disassembly mechanism. *Nat. Commun.* 6:7202. https://doi.org/10.1038/ncomms8202

Khatau, S.B., D.-H. Kim, C.M. Hale, R.J. Bloom, and D. Wirtz. 2010. The perinuclear actin cap in health and disease. *Nucleus.* 1:337–342. https://doi.org/10.4161/nucl.1.4.12331

Kim, J.-K., A. Louhghalam, G. Lee, B.W. Schafer, D. Wirtz, and D.-H. Kim. 2017. Nuclear lamin A/C harnesses the perinuclear apical actin cables to protect nuclear morphology. *Nat. Commun.* 8:2123. https://doi.org/10.1038/s41467-017-02217-5

Kuhn, T.B., and J.R. Bamburg. 2008. Tropomyosin and ADF/cofilin as collaborators and competitors. *Adv. Exp. Med. Biol.* 644:232–249. https://doi.org/10.1007/978-0-387-85766-4_18

Kuhns, D.B., D.L. Fink, U. Choi, C. Sweeney, K. Lau, D.L. Priel, D. Riva, L. Mendez, G. Uzel, A.F. Freeman, et al. 2016. Cytoskeletal abnormalities and neutrophil dysfunction in WDR1 deficiency. *Blood.* 128:2135–2143. https://doi.org/10.1182/blood-2016-03-706028

Lam, P.Y., S. Mangos, J.M. Green, J. Reiser, and A. Huttenlocher. 2015. In vivo imaging and characterization of actin microridges. *PLoS One.* 10: e0115639. https://doi.org/10.1371/journal.pone.0115639

Lammerding, J., and K. Wolf. 2016. Nuclear envelope rupture: Actin fibers are putting the squeeze on the nucleus. *J. Cell Biol.* 215:5–8. https://doi.org/10.1083/jcb.201609102

Le Guyader, D., M.J. Redd, E. Colucci-Guyon, E. Murayama, K. Kissa, V. Briolat, E. Mordelet, A. Zapata, H. Shinomiya, and P. Herbomel. 2008. Origins and unconventional behavior of neutrophils in developing zebrafish. *Blood.* 111:132–141. https://doi.org/10.1182/blood-2007-06-095398

Loynes, C.A., J.S. Martin, A. Robertson, D.M.I. Trushell, P.W. Ingham, M.K.B. Whyte, and S.A. Renshaw. 2010. Pivotal Advance: Pharmacological manipulation of inflammation resolution during spontaneously resolving tissue neutrophilia in the zebrafish. *J. Leukoc. Biol.* 87:203–212. https://doi.org/10.1189/jlb.0409255

Maekawa, M., T. Ishizaki, S. Boku, N. Watanabe, A. Fujita, A. Iwamatsu, T. Obinata, K. Ohashi, K. Mizuno, and S. Narumiya. 1999. Signaling from Rho to the actin cytoskeleton through protein kinases ROCK and LIM-kinase. *Science.* 285:895–898. https://doi.org/10.1126/science.285.5429.895

McMenamin, S., S. Reinsch, and G. Conway. 2003. Direct comparison of common fixation methods for preservation of microtubules in zebrafish embryos. *Biotechniques.* 34:468–472. https://doi.org/10.2144/03343bm03

Miller, M.E., F.A. Oski, and M.B. Harris. 1971. Lazy-leucocyte syndrome. A new disorder of neutrophil function. *Lancet.* 1:665–669. https://doi.org/10.1016/S0140-6736(71)92679-1

Moulding, D.A., M.P. Blundell, D.G. Spiller, M.R.H. White, G.O. Cory, Y. Calle, H. Kempski, J. Sinclair, P.J. Ancliff, C. Kinnon, et al. 2007. Unregulated actin polymerization by WASp causes defects of mitosis and cytokinesis in X-linked neutropenia. *J. Exp. Med.* 204:2213–2224. https://doi.org/10.1084/jem.20062324

Moulding, D.A., E. Moeendarbary, L. Valon, J. Record, G.T. Charras, and A.J. Thrasher. 2012. Excess F-actin mechanically impedes mitosis leading to cytokinesis failure in X-linked neutropenia by exceeding Aurora B kinase error correction capacity. *Blood.* 120:3803–3811. https://doi.org/10.1182/blood-2012-03-419663

Nadkarni, A.V., and W.M. Brieher. 2014. Aip1 destabilizes cofilin-saturated actin filaments by severing and accelerating monomer dissociation from ends. *Curr. Biol.* 24:2749–2757. https://doi.org/10.1016/j.cub.2014.09.048

Nunoi, H., T. Yamazaki, and S. Kanegasaki. 2001. Neutrophil cytoskeletal disease. *Int. J. Hematol.* 74:119–124. https://doi.org/10.1007/BF02981993

Ojeda, V., A. Castro-Castro, and X.R. Bustelo. 2014. Coronin1 proteins dictate rac1 intracellular dynamics and cytoskeletal output. *Mol. Cell. Biol.* 34:3388–3406. https://doi.org/10.1128/MCB.00347-14

Olins, A.L., M. Zwerger, H. Herrmann, H. Zentgraf, A.J. Simon, M. Monestier, and D.E. Olins. 2008. The human granulocyte nucleus: Unusual nuclear envelope and heterochromatin composition. *Eur. J. Cell Biol.* 87:279–290. https://doi.org/10.1016/j.ejcb.2008.02.007

Olins, A.L., T.V. Hoang, M. Zwerger, H. Herrmann, H. Zentgraf, A.A. Noegel, I. Karakesisoglou, D. Hodzic, and D.E. Olins. 2009. The LINC-less granulocyte nucleus. *Eur. J. Cell Biol.* 88:203–214. https://doi.org/10.1016/j.ejcb.2008.10.001

Ono, S. 2003. Regulation of actin filament dynamics by actin depolymerizing factor/cofilin and actin-interacting protein 1: new blades for twisted filaments. *Biochemistry.* 42:13363–13370. https://doi.org/10.1021/bi034600x

Ono, S. (2018). Functions of actin-interacting protein 1 (AIP1)/WD repeat protein 1 (WDR1) in actin filament dynamics and cytoskeletal regulation. *Biochem. Biophys. Res. Commun.*506:315–322.

Palais, R.A., M.A. Liew, and C.T. Wittwer. 2005. Quantitative heteroduplex analysis for single nucleotide polymorphism genotyping. *Anal. Biochem.* 346:167–175. https://doi.org/10.1016/j.ab.2005.08.010

Pfajfer, L., N.K. Mair, R. Jiménez-Heredia, F. Genel, N. Gulez, Ö. Ardeniz, B. Hoeger, S.K. Bal, C. Madritsch, A. Kalinichenko, et al. 2018. Mutations affecting the actin regulator WD repeat-containing protein 1 lead to aberrant lymphoid immunity. *J. Allergy Clin. Immunol.* 142:1589–1604.e11. https://doi.org/10.1016/j.jaci.2018.04.023

Raab, M., M. Gentili, H. de Belly, H.R. Thiam, P. Vargas, A.J. Jimenez, F. Lautenschlaeger, R. Voituriez, A.M. Lennon-Duménil, N. Manel, and M. Piel. 2016. ESCRT III repairs nuclear envelope ruptures during cell migration to limit DNA damage and cell death. *Science.* 352:359–362. https://doi.org/10.1126/science.aad7611

Renshaw, S.A., C.A. Loynes, D.M.I. Trushell, S. Elworthy, P.W. Ingham, and M.K.B. Whyte. 2006. A transgenic zebrafish model of neutrophilic inflammation. *Blood.* 108:3976–3978. https://doi.org/10.1182/blood-2006-05-024075

Rowat, A.C., D.E. Jaalouk, M. Zwerger, W.L. Ung, I.A. Eydelnant, D.E. Olins, A.L. Olins, H. Herrmann, D.A. Weitz, and J. Lammerding. 2013. Nuclear envelope composition determines the ability of neutrophil-type cells to passage through micron-scale constrictions. *J. Biol. Chem.* 288:8610–8618. https://doi.org/10.1074/jbc.M112.441535

Sarris, M., J.-B. Masson, D. Maurin, L.M. Van der Aa, P. Boudinot, H. Lortat-Jacob, and P. Herbomel. 2012. Inflammatory chemokines direct and restrict leukocyte migration within live tissues as glycan-bound gradients. *Curr. Biol.* 22:2375–2382. https://doi.org/10.1016/j.cub.2012.11.018

Shelef, M.A., S. Tauzin, and A. Huttenlocher. 2013. Neutrophil migration: moving from zebrafish models to human autoimmunity. *Immunol. Rev.* 256:269–281. https://doi.org/10.1111/imr.12124

Singh, M., C.R. Hunt, R.K. Pandita, R. Kumar, C.-R. Yang, N. Horikoshi, R. Bachoo, S. Serag, M.D. Story, J.W. Shay, et al. 2013a. Lamin A/C depletion enhances DNA damage-induced stalled replication fork arrest. *Mol. Cell. Biol.* 33:1210–1222. https://doi.org/10.1128/MCB.01676-12

Singh, S.K., S. Sethi, S. Aravamudhan, M. Krüger, and C. Grabher. 2013b. Proteome mapping of adult zebrafish marrow neutrophils reveals partial cross species conservation to human peripheral neutrophils. *PLoS One.* 8:e73998. https://doi.org/10.1371/journal.pone.0073998

Standing, A.S.I., D. Malinova, Y. Hong, J. Record, D. Moulding, M.P. Blundell, K. Nowak, H. Jones, E. Omoyinmi, K.C. Gilmour, et al. 2017. Autoinflammatory periodic fever, immunodeficiency, and thrombocytopenia (PFIT) caused by mutation in actin-regulatory gene WDR1. *J. Exp. Med.* 214:59–71. https://doi.org/10.1084/jem.20161228

Strzyz, P.J., H.O. Lee, J. Sidhaye, I.P. Weber, L.C. Leung, and C. Norden. 2015. Interkinetic nuclear migration is centrosome independent and ensures apical cell division to maintain tissue integrity. *Dev. Cell.* 32:203–219. https://doi.org/10.1016/j.devcel.2014.12.001

Svoboda, K.R., A.E. Linares, and A.B. Ribera. 2001. Activity regulates programmed cell death of zebrafish Rohon-Beard neurons. *Development.* 128:3511–3520.

Thiam, H.-R., P. Vargas, N. Carpi, C.L. Crespo, M. Raab, E. Terriac, M.C. King, J. Jacobelli, A.S. Alberts, T. Stradal, et al. 2016. Perinuclear Arp2/3-driven actin polymerization enables nuclear deformation to facilitate cell migration through complex environments. *Nat. Commun.* 7:10997. https://doi.org/10.1038/ncomms10997

Ungricht, R., and U. Kutay. 2017. Mechanisms and functions of nuclear envelope remodelling. *Nat. Rev. Mol. Cell Biol.* 18:229–245. https://doi.org/10.1038/nrm.2016.153

Voegtli, W.C., A.Y. Madrona, and D.K. Wilson. 2003. The structure of Aip1p, a WD repeat protein that regulates Cofilin-mediated actin depolymerization. *J. Biol. Chem.* 278:34373–34379. https://doi.org/10.1074/jbc.M302773200

Weiser, D.C., and D. Kimelman. 2012. Analysis of cell shape and polarity during zebrafish gastrulation. *Methods Mol. Biol.* 839:53–68. https://doi.org/10.1007/978-1-61779-510-7_5

Westerfield, M. 2000. *The zebrafish book. A guide for the laboratory use of zebrafish (Danio rerio).* Univ. of Oregon Press, Eugene, OR.

Wiggan, O., A.E. Shaw, J.G. DeLuca, and J.R. Bamburg. 2012. ADF/cofilin regulates actomyosin assembly through competitive inhibition of myosin II binding to F-actin. *Dev. Cell.* 22:530–543. https://doi.org/10.1016/j.devcel.2011.12.026

Xiao, Y., H. Ma, P. Wan, D. Qin, X. Wang, X. Zhang, Y. Xiang, W. Liu, J. Chen, Z. Yi, and L. Li. 2017. Trp-Asp (WD) Repeat Domain 1 Is Essential for Mouse Peri-implantation Development and Regulates Cofilin Phosphorylation. *J. Biol. Chem.* 292:1438–1448. https://doi.org/10.1074/jbc.M116.759886

Yoo, S.K., Q. Deng, P.J. Cavnar, Y.I. Wu, K.M. Hahn, and A. Huttenlocher. 2010. Differential regulation of protrusion and polarity by PI3K during neutrophil motility in live zebrafish. *Dev. Cell.* 18:226–236. https://doi.org/10.1016/j.devcel.2009.11.015

Yoo, S.K., P.-Y. Lam, M.R. Eichelberg, L. Zasadil, W.M. Bement, and A. Huttenlocher. 2012. The role of microtubules in neutrophil polarity and migration in live zebrafish. *J. Cell Sci.* 125:5702–5710. https://doi.org/10.1242/jcs.108324

Yuan, B., P. Wan, D. Chu, J. Nie, Y. Cao, W. Luo, S. Lu, J. Chen, and Z. Yang. 2014. A cardiomyocyte-specific Wdr1 knockout demonstrates essential functional roles for actin disassembly during myocardial growth and maintenance in mice. *Am. J. Pathol.* 184:1967–1980. https://doi.org/10.1016/j.ajpath.2014.04.007